f-band ferromagnetism in the periodic Anderson model - a modified alloy analogy

2000 J. Phys.: Condens. Matter 12 7463

(http://iopscience.iop.org/0953-8984/12/33/313)

J. Phys.: Condens. Matter **12** (2000) 7463–7480. Printed in the UK PII: S0953-8984(00)13073-5

f-band ferromagnetism in the periodic Anderson model—a modified alloy analogy

G G Reddy†, D Meyer‡, S Schwieger‡, A Ramakanth† and W Nolting‡

† Department of Physics, Kakatiya University, Warangal-506009, India
‡ Institut für Physik, Humboldt-Universität zu Berlin, D-10115 Berlin, Germany

Received 5 April 2000

Abstract. We introduce a new approximation scheme for the periodic Anderson model (PAM). The modified alloy approximation represents an optimum alloy approximation for the strong-coupling limit, which can be solved within the coherent-potential-approximation formalism. Zero-temperature and finite-temperature phase diagrams are presented for the PAM in the intermediate-valence regime. The diversity of magnetic properties accessible by variation of the system parameters can be studied by means of quasiparticle densities of states: the conduction band couples either ferromagnetically or antiferromagnetically to the f levels. A finite hybridization is a necessary precondition for ferromagnetism. However, too strong a hybridization generally suppresses ferromagnetism, but can for certain system parameters also lead to a semi-metallic state with unusual magnetic properties. By comparing with the spectral density approximation, the influence of quasiparticle damping can be examined.

1. Introduction

Correlated electron systems have come to occupy centre stage in both theory and experiment in condensed matter physics. There is a general consensus that strong electron correlations play a decisive role in a variety of phenomena such as magnetism, heavy fermions, high-temperature superconductivity, and colossal magnetoresistance. Real systems that display these phenomena include transition metals (3d), alloys and compounds, as well as rare-earth (4f) systems (metals, insulators), in particular cuprates, manganites, and Ce compounds. There is intense activity both theoretically and experimentally focused on isolating the essential interactions responsible for these phenomena. In this process, several model systems are being studied which are expected to at least qualitatively mimic the actual systems in some region of the parameter space. One of the most widely used models which brings out the role of electron correlations while also taking into account the interplay of two different types of electron, one highly localized and the other quasifree, is the well-known Anderson model [1]. One distinguishes the 'single-impurity Anderson model' (SIAM), if the system of uncorrelated conduction electrons hybridizes with a single localized state, and the 'periodic Anderson model' (PAM), if the hybridization takes place with a periodic lattice of localized states. For the SIAM, many exact results have been obtained, e.g. by using Bethe-*ansatz* [2] or renormalization group theory [3]. Very recently the SIAM has gained new impetus in connection with the 'dynamical mean-field theory' [4–6] which exploits the fact that in infinite lattice dimensions theoretical lattice models like the Hubbard model can be mapped onto single-impurity models such as the SIAM. Numerically essentially exact methods such as the exact diagonalization of small systems, quantum Monte Carlo calculations, and numerical renormalization group theory [6, 7] have

0953-8984/00/337463+18$30.00

provided further insight into the physics of the model. However, since these numerical methods are restricted by certain limitations, reliable analytical approaches remain to be established [8].

The situation is less satisfactory in the case of the PAM. Even though there exist a number of approximate schemes for different parameter constellations, referring to the so-called heavy-fermion, intermediate-valence, and Kondo regimes, there is still a need for further improvement and extension. This need has acquired additional urgency in view of the fact that for the parameter space corresponding to strongly correlated low-lying localized states, the PAM can be mapped [9] onto the Kondo-lattice model [10] which is of great current interest, e.g. with reference to the extraordinary physical properties of the manganites [11].

Recently we proposed a new approximation scheme [12] which is based on a mapping of the PAM onto an effective Hubbard model. The parameters of the Hubbard model are such that they correspond to the strong-coupling limit. Therefore we could exploit a reliable approximate theory, valid in the strong-coupling limit. One such theory is the 'spectral density approach' (SDA) [13–15]. Its main advantages are the physically simple concept and the non-perturbative character. In this scheme we have studied the magnetic $T = 0$ phase diagram of the PAM as well as its finite-temperature magnetic properties. The SDA, however, exhibits a major limitation concerning quasiparticle damping. By *ansatz*, the SDA self-energy is a real quantity, thus neglecting from the very outset effects due to the finite lifetimes of the quasiparticles. How quasiparticle damping influences the magnetic stability in the PAM is an interesting and important question, which was been left open by our previous theory [12]. It is the main aim of the present study to close this gap.

One conceptually simple method that is able to provide complex self-energies is the 'coherent potential approximation' (CPA) [16]. In order to apply the CPA to the PAM, we have to construct an alloy analogy. This requires the determination of the energy levels and the concentrations of the components of the fictitious alloy. Within the conventional alloy analogy (AA) treatment due to Hubbard [17], these are obtained by referring to the atomic limit. For an application to the PAM, see e.g. [18, 19]. However, this choice is by no means predetermined. On the contrary, it can be shown that it is in fact not the best *ansatz*. It is known that the CPA becomes an exact procedure for infinite lattice dimensions ($d = \infty$), where the inherent single-site aspect of the CPA is rigorous [20]. However, the CPA solution of the AA for the $d = \infty$ Hubbard model violates the exactly known strong-coupling-behaviour requirement [21] and also does not reproduce the weak-coupling results of second-order perturbation theory [22, 23]. Furthermore, it contradicts exact high-energy expansions [24]. So we have to conclude that the conventional AA, which starts from the atomic limit solution, is not the most convenient alloy analogy. In this paper we therefore derive a 'modified alloy analogy' (MAA), which was recently introduced for the Hubbard model [24, 25], for the PAM. This method substantially improves on the AA *ansatz* by deriving an appropriate alloy analogy from exact high-energy expansions of the single-electron Green function and the self-energy. This procedure guarantees the correct strong-coupling behaviour relevant for the PAM. On the way to deriving the MAA, the above-mentioned SDA can easily be re-derived without the necessity of introducing the effective Hubbard model as was done before [12]. It turns out that the 'atomic levels' of the fictitious alloy constituents are nothing but the SDA quasiparticle energies in the zero-bandwidth limit. Similarly the 'concentrations' agree with the SDA spectral weights in this limit. The MAA thus promises to retain the advantages of the SDA while simultaneously improving the method by incorporating quasiparticle damping. The SDA energies and spectral weights contain non-trivial thermodynamic expectation values which have to be determined self-consistently. Through them, the itineracy of the $-\sigma$-electrons, which define the fictitious alloy for the propagating σ-electrons, comes into play, at least to a certain degree. The neglect of this itineracy is a well-known shortcoming of the conventional AA.

The paper is organized as follows. In the next section the PAM and its many-body problem are formulated. An approximate solution by use of the MAA scheme is then developed in section 3. Section 4 is devoted to a presentation and discussion of the results concerning the magnetic properties of the PAM. The paper ends with some concluding remarks.

2. The model Hamiltonian and its many-body problem

The starting point is the periodic Anderson Hamiltonian

$$H = \sum_{ij\sigma}(T_{ij} - \mu)s^{\dagger}_{i\sigma}s_{j\sigma} + \sum_{i\sigma}(e_{\mathrm{f}} - \mu)f^{\dagger}_{i\sigma}f_{i\sigma} + V\sum_{i\sigma}(f^{\dagger}_{i\sigma}s_{i\sigma} + s^{\dagger}_{i\sigma}f_{i\sigma}) + \frac{1}{2}U\sum_{i\sigma}n^{(\mathrm{f})}_{i\sigma}n^{(\mathrm{f})}_{i-\sigma}. \tag{1}$$

$s_{i\sigma}$ ($f_{i\sigma}$) and $s^{\dagger}_{i\sigma}$ ($f^{\dagger}_{i\sigma}$) are, respectively, the annihilation and the creation operators for an electron in a non-degenerate conduction band (localized f state), and

$$n^{(\mathrm{f})}_{i\sigma} = f^{\dagger}_{i\sigma}f_{i\sigma} \tag{2}$$

is the spin-dependent occupation number operator for the f state. The index i refers to the respective lattice site; $\sigma = \{\uparrow, \downarrow\}$ is the spin projection. The hopping integral T_{ij}:

$$T_{ij} = \frac{1}{N}\sum_{\boldsymbol{k}} \mathrm{e}^{-\mathrm{i}\boldsymbol{k}\cdot(\boldsymbol{R}_i - \boldsymbol{R}_j)}\epsilon(\boldsymbol{k}) \tag{3}$$

describes the propagation of a band electron from site $\boldsymbol{R}_j$ to site $\boldsymbol{R}_i$. $\epsilon(\boldsymbol{k})$ is the free Bloch energy, while e_{f} denotes the position of the non-degenerate f level. We choose the energy zero to coincide with the centre of gravity of the unperturbed conduction band:

$$T_{ii} = \frac{1}{N}\sum_{\boldsymbol{k}}\epsilon(\boldsymbol{k}) \stackrel{!}{=} 0. \tag{4}$$

U is the intra-atomic Coulomb repulsion between f electrons. The hybridization V is taken as a real and $\boldsymbol{k}$-independent local matrix element; μ is the chemical potential.

Let us start with the retarded single-s-electron and single-f-electron Zubarev Green's functions:

$$G^{(\mathrm{f})}_{ij\sigma}(E) = \langle\langle f_{i\sigma}; f^{\dagger}_{j\sigma}\rangle\rangle \qquad G^{(\mathrm{s})}_{ij\sigma}(E) = \langle\langle s_{i\sigma}; s^{\dagger}_{j\sigma}\rangle\rangle \tag{5}$$

$$G^{(\mathrm{f,s})}_{\boldsymbol{k}\sigma} = \frac{1}{N}\sum_{\boldsymbol{k}}\mathrm{e}^{\mathrm{i}\boldsymbol{k}\cdot(\boldsymbol{R}_i - \boldsymbol{R}_j)}G^{(\mathrm{f,s})}_{ij\sigma}(E). \tag{6}$$

The equations of motion are easily derived and formally solved:

$$G^{(\mathrm{s})}_{\boldsymbol{k}\sigma}(E) = \hbar\frac{E - (e_{\mathrm{f}} - \mu) - \Sigma_{\boldsymbol{k}\sigma}(E)}{(E - (e_{\mathrm{f}} - \mu) - \Sigma_{\boldsymbol{k}\sigma}(E))(E - (\epsilon(\boldsymbol{k}) - \mu)) - V^2} \tag{7}$$

$$G^{(\mathrm{f})}_{\boldsymbol{k}\sigma}(E) = \hbar\Big/\left(E - (e_{\mathrm{f}} - \mu) - \frac{V^2}{E - (\epsilon(\boldsymbol{k}) - \mu)} - \Sigma_{\boldsymbol{k}\sigma}(E)\right) \tag{8}$$

where the self-energy $\Sigma_{\boldsymbol{k}\sigma}(E)$ has been introduced via

$$\Sigma_{\boldsymbol{k}\sigma}(E)G^{(\mathrm{f})}_{\boldsymbol{k}\sigma}(E) = U\frac{1}{N}\sum_{\boldsymbol{p},\boldsymbol{q}}\langle\langle f^{\dagger}_{\boldsymbol{p}-\sigma}f_{\boldsymbol{q}-\sigma}f_{\boldsymbol{p}+\boldsymbol{k}-\boldsymbol{q}\sigma}; f^{\dagger}_{\boldsymbol{k}\sigma}\rangle\rangle. \tag{9}$$

Obviously the explicit problem is solved as soon as we have found a solution for the self-energy. The f- and s-quasiparticle densities of states (QDOS) are given by

$$\rho_\sigma^{(\mathrm{s})}(E) = -\frac{1}{\pi\hbar N}\sum_{\boldsymbol{k}} \Im G_{\boldsymbol{k}\sigma}^{(\mathrm{s})}(E-\mu+\mathrm{i}0^+) \tag{10}$$

$$\rho_\sigma^{(\mathrm{f})}(E) = -\frac{1}{\pi\hbar N}\sum_{\boldsymbol{k}} \Im G_{\boldsymbol{k}\sigma}^{(\mathrm{f})}(E-\mu+\mathrm{i}0^+) \tag{11}$$

and determine the spin-dependent average occupation numbers $n_\sigma^{(\mathrm{s,f})}$, which we need to construct the magnetic phase diagram of the PAM:

$$n_\sigma^{(\mathrm{s})} = \langle s_{i\sigma}^\dagger s_{i\sigma}\rangle = \int_{-\infty}^{+\infty} \mathrm{d}E\ f_-(E)\rho_\sigma^{(\mathrm{s})}(E) \tag{12}$$

$$n_\sigma^{(\mathrm{f})} = \langle f_{i\sigma}^\dagger f_{i\sigma}\rangle = \int_{-\infty}^{+\infty} \mathrm{d}E\ f_-(E)\rho_\sigma^{(\mathrm{f})}(E). \tag{13}$$

3. The modified alloy analogy

A standard method for solving many-body problems such as that posed by the PAM Hamiltonian (1) is the CPA [16]. As a single-site approximation, the resulting f-electron self-energy will be local, i.e. $\boldsymbol{k}$-independent. If we apply this method here, we have to solve the following equation self-consistently:

$$0 = \sum_{p=1}^{n} x_{p\sigma}\frac{E_{p\sigma}-\Sigma_\sigma(E)-e_\mathrm{f}}{1-(1/\hbar)G_{ii\sigma}^{(\mathrm{f})}(E)(E_{p\rho}-\Sigma_\sigma(E)-e_\mathrm{f})} \tag{14}$$

$$G_{ii\sigma}^{(\mathrm{f})}(E) = \frac{1}{N}\sum_{\boldsymbol{k}} G_{\boldsymbol{k}\sigma}^{(\mathrm{f})}(E) \qquad \Sigma_\sigma(E) = \frac{1}{N}\sum_{\boldsymbol{k}}\Sigma_{\boldsymbol{k}\sigma}(E). \tag{15}$$

The solution of (14) needs one to fix the alloy analogy, i.e. the 'atomic levels' $E_{p\sigma}$ and the 'concentrations' $x_{p\sigma}$ of the n constituents of the fictitious alloy. Since the dominant features of the correlated f level in the PAM are the two charge excitations separated by U, the number of 'alloyed' components n is set to two. The conventional alloy analogy (AA) uses the $V=0$ limit ('atomic' limit) of the PAM to determine $E_{p\sigma}$ and $x_{p\sigma}$ [18, 19]:

$$\begin{aligned} E_{1\sigma}^{(\mathrm{AA})} &= e_\mathrm{f} & x_{1\sigma}^{(\mathrm{AA})} &= 1-n_{-\sigma}^{(\mathrm{f})} \\ E_{2\sigma}^{(\mathrm{AA})} &= e_\mathrm{f}+U & x_{2\sigma}^{(\mathrm{AA})} &= n_{-\sigma}^{(\mathrm{f})}. \end{aligned} \tag{16}$$

The result violates the weak as well as the strong coupling behaviour and, as for the Hubbard model, prohibits spontaneous magnetism [18, 24, 26, 27]. In particular, the strong-coupling behaviour appears to be crucial for ferromagnetism. On the other hand, the choice (16) is not at all predetermined. We propose another way to establish the 'best alloy analogy'. Correct strong-coupling behaviour is guaranteed by fulfilment of the high-energy expansion of the relevant Green functions and self-energies [24]. The decisive ingredients for proper high-energy expansions are the local spectral moments:

$$\begin{aligned} M_\sigma^{(n)} &= \frac{1}{N}\sum_{\boldsymbol{k}} M_{\boldsymbol{k}\sigma}^{(n)} \qquad n=0,1,2,\ldots \\ M_{\boldsymbol{k}\sigma}^{(n)} &= \frac{1}{\hbar}\int \mathrm{d}E\ E^n S_{\boldsymbol{k}\sigma}(E). \end{aligned} \tag{17}$$

$S_{\boldsymbol{k}\sigma}(E)$ is the f-electron spectral density:

$$S_{\boldsymbol{k}\sigma}(E) = -\frac{1}{\pi}\Im G_{\boldsymbol{k}\sigma}^{(\mathrm{f})}(E+\mathrm{i}0^+). \tag{18}$$

The moments can be calculated independently of the required spectral density:

$$M_{k\sigma}^{(n)} = \langle [\underbrace{[\ldots[f_{k\sigma}, H]_-, \ldots, H]_-}_{n-\text{fold commutator}}, f_{k\sigma}^\dagger]_+ \rangle. \tag{19}$$

$[\ldots,\ldots]_-$ denotes the commutator and $[\ldots,\ldots]_+$ denotes the anticommutator. For the Green function (5) we can write

$$G_{k\sigma}^{(\mathrm{f})}(E) = \int_+^\infty -\infty \mathrm{d}E' \, \frac{S_{k\sigma}(E')}{E - E'} = \hbar \sum_{n=0}^{\infty} \frac{M_{k\sigma}^{(n)}}{E^{n+1}}. \tag{20}$$

To solve the CPA equation (14), we only need the local spectral moments, which are found to be

$$\begin{aligned}
M_\sigma^{(0)} &= 1 \\
M_\sigma^{(1)} &= e_\mathrm{f} + U n_{-\sigma}^{(\mathrm{f})} \\
M_\sigma^{(2)} &= e_\mathrm{f}^2 + 2e_\mathrm{f} U n_{-\sigma}^{(\mathrm{f})} + U^2 n_{-\sigma}^{(\mathrm{f})} + V^2 \\
M_\sigma^{(3)} &= e_\mathrm{f}^3 + 3e_\mathrm{f}^2 U n_{-\sigma}^{(\mathrm{f})} + U^2 e_\mathrm{f}(2n_{-\sigma}^{(\mathrm{f})} + n_{-\sigma}^{(\mathrm{f})^2}) + U^3 n_{-\sigma}^{(\mathrm{f})} + \\
&\quad + V^2(2e_\mathrm{f} + 2U n_{-\sigma}^{(\mathrm{f})} + T_{ii}) + U^2 n_{-\sigma}^{(\mathrm{f})}(1 - n_{-\sigma}^{(\mathrm{f})}) B_{-\sigma}.
\end{aligned} \tag{21}$$

From (8) we get the corresponding expansion for the self-energy:

$$\Sigma_{k\sigma}(E) = \sum_{n=0}^{\infty} \frac{C_{k\sigma}^{(n)}}{E^n} \qquad \Sigma_\sigma(E) = \frac{1}{N} \sum_{k} \Sigma_{k\sigma}(E) \tag{22}$$

with the local coefficients

$$\begin{aligned}
C_\sigma^{(0)} &= U n_{-\sigma}^{(\mathrm{f})} \\
C_\sigma^{(1)} &= U^2 n_{-\sigma}^{(\mathrm{f})}(1 - n_{-\sigma}^{(\mathrm{f})}) \\
C_\sigma^{(2)} &= U^2 n_{-\sigma}^{(\mathrm{f})}(1 - n_{-\sigma}^{(\mathrm{f})})(B_{-\sigma} + U(1 - n_{-\sigma}^{(\mathrm{f})})).
\end{aligned} \tag{23}$$

Surprisingly, the hybridization V does not explicitly appear in the $C_\sigma^{(n)}$. The contributions via the moments (21) are exactly cancelled by those from the term $V^2/(E - (\epsilon(k) - \mu))$ in (8).

By use of (20) and (22), we now expand the CPA equation (14) in powers of $1/E$. Comparison of the coefficients of the $1/E^n$ terms up to $n = 3$ yields the following set of four equations for the four unknown quantities $E_{(1,2)\sigma}$ and $x_{(1,2)\sigma}$:

$$\begin{aligned}
&\sum_{p=1}^{2} x_{p\sigma} = 1 \\
&\sum_{p=1}^{2} x_{p\sigma}(E_{p\sigma} - e_\mathrm{f}) = U n_{-\sigma}^{(\mathrm{f})} \\
&\sum_{p=1}^{2} x_{p\sigma}(E_{p\sigma} - e_\mathrm{f})^2 = U^2 n_{-\sigma}^{(\mathrm{f})} \\
&\sum_{p=1}^{2} x_{p\sigma}(E_{p\sigma} - e_\mathrm{f})^3 = U^3 n_{-\sigma}^{(\mathrm{f})} + U^2 n_{-\sigma}^{(\mathrm{f})}(1 - n_{-\sigma}^{(\mathrm{f})})(B_{-\sigma} - e_\mathrm{f}).
\end{aligned} \tag{24}$$

We now use equations (24) to fix the 'optimum' alloy analogy. After simple manipulations we obtain

$$\begin{aligned}
E_{1,2\sigma} &= \frac{1}{2}\Big[B_{-\sigma} + U + e_\mathrm{f} \pm \sqrt{(B_{-\sigma} + U - e_\mathrm{f})^2 + 4U n_{-\sigma}^{(\mathrm{f})}(e_\mathrm{f} - B_{-\sigma})}\Big] \\
x_{1\sigma} &= \frac{E_{2\sigma} - e_\mathrm{f} - U n_{-\sigma}^{(\mathrm{f})}}{E_{2\sigma} - E_{1\sigma}} = 1 - x_{2\sigma}.
\end{aligned} \tag{25}$$

The decisive element for the ongoing procedure is the 'higher' correlation function $B_{-\sigma}$:

$$n^{(\mathrm{f})}_{-\sigma}(1-n^{(\mathrm{f})}_{-\sigma})(B_{-\sigma}-e_{\mathrm{f}}) = V\langle f^{\dagger}_{i-\sigma}s_{i-\sigma}(2n^{(\mathrm{f})}_{i\sigma}-1)\rangle. \tag{26}$$

It has been demonstrated in previous works [13–15,24] that its analogue has a decisive influence on the stability of the spontaneous magnetism in the Hubbard model. We believe that it plays a similarly important role for ferromagnetism in the PAM [12,28]. In spite of the fact that it is a 'higher' correlation function, it can be rigorously expressed using single-electron terms [13]:

$$n^{(\mathrm{f})}_{-\sigma}(1-n^{(\mathrm{f})}_{-\sigma})(B_{-\sigma}-e_{\mathrm{f}}) = -\frac{1}{\pi\hbar}\Im\int_{-\infty}^{+\infty}\mathrm{d}E\ f_{-}(E)\left(\frac{2}{U}\Sigma_{\sigma}(E)-1\right)$$
$$\times\,[(E-(e_{\mathrm{f}}-\mu)-\Sigma_{\sigma}(E))G^{(\mathrm{f})}_{ii\sigma}(E)-\hbar]. \tag{27}$$

With the fictitious alloy (25), we enter the CPA equation (14). The theory is now complete. The equations (14), (15), (8), (27), and (13), together with (25), build a closed system of equations which can be solved self-consistently for the self-energy $\Sigma_{\sigma}(E)$. Note that the only $\boldsymbol{k}$-dependence that comes into play in (8) arises via the formal solution of the equation of motion. The dependence on $\boldsymbol{k}$ is therefore strictly an $\epsilon(\boldsymbol{k})$ dependence, so all k-summations can be replaced by simpler energy integration over the 'free' Bloch density of states:

$$\rho_0(E) = (1/N)\sum_{\boldsymbol{k}}\delta(E-\epsilon(\boldsymbol{k}))$$

which has to be considered as a model parameter:

$$G^{(\mathrm{f})}_{ii\sigma}(E) = \hbar\int_{-\infty}^{+\infty}\mathrm{d}x\ \rho_0(x)\Big/\left(E-(e_{\mathrm{f}}-\mu)-\frac{V^2}{E-(x-\mu)}-\Sigma_{\sigma}(E)\right). \tag{28}$$

Let us comment on the modified alloy analogy (25) and its differences from the conventional AA (16): within the AA, the σ–f electron is propagating through a fictitious alloy where one component is represented by lattice sites with no $-\sigma$-electron present, and the other component is represented by lattice sites which are occupied by one $-\sigma$-electron. This approach therefore completely neglects the hybridization between the f levels and the conduction band. For calculating the self-energy, the $-\sigma$–f electrons are frozen; any exchange with the conduction band is eliminated. This excludes the possibility of magnetic order in the system. How can this drawback be circumvented? It is clear that the PAM will always be considered to belong to the strong-coupling regime (large U). Two well-separated excitation peaks will therefore be expected in the f-electron quasiparticle density of states. The above-described *ansatz* for fitting the positions and weights of these to an exact $1/E$ expansion of the Green function seems the most plausible one, since these charge excitation peaks are themselves high-energy features. It is noteworthy that all differences induced thereby between the MAA and the AA are due to the hybridization between f and s levels. It can be seen in equation (26) that in the limit of vanishing hybridization ($V=0$), $B_{-\sigma}=e_{\mathrm{f}}$ holds and equations (25) reduce to the conventional alloy analogy (16). However, for finite hybridization, $B_{-\sigma}$ and $n^{(\mathrm{f})}_{-\sigma}$ are to be determined self-consistently by (27) and (13), respectively, possibly providing the alloy energies and concentrations with an explicit spin dependence. In each step of the CPA iteration, $B_{-\sigma}$ and $n^{(\mathrm{f})}_{-\sigma}$ may change, and so can the underlying fictitious alloy. Equation (26) makes it clear that the inclusion of $B_{-\sigma}$ accounts to a certain degree for the hybridization of $-\sigma$–f electrons with the conduction band and therefore also for their effective itineracy which is completely neglected in the conventional alloy analogy (16).

Before further discussing the MAA, let us remind the reader of the already mentioned spectral density approximation (SDA). In a previous work, this theory was derived via mapping of the PAM onto an effective-medium Hubbard model [12]. Within this effective Hubbard model, the SDA is justified in the strong-coupling limit where the positions and spectral weights

obtained for the lower and upper Hubbard band coincide with exact results up to the order $1/U$ [21]. At this point it is worth noting that exactly the same results as in reference [12] can also be obtained by adapting the concept of the SDA directly to the PAM, which is possible and straightforward from the above-presented results. Motivated by the solution for the 'atomic' limit ($V = 0$), we make the following *ansatz* for the self-energy:

$$\Sigma_\sigma(E) = \alpha_{1\sigma}\frac{E - \alpha_{2\sigma}}{E - \alpha_{3\sigma}}. \tag{29}$$

The coefficients of this *ansatz* can now be fitted in such a way that the high-energy expansion of the self-energy, equation (22), with the coefficients (23), is obeyed. One readily arrives at

$$\Sigma_\sigma^{(\mathrm{SDA})}(E) = \frac{U n_{-\sigma}^{(\mathrm{f})}(E - B_{-\sigma})}{E - B_{-\sigma} - U(1 - n_{-\sigma}^{(\mathrm{f})})} \tag{30}$$

which, together with equations (28), (27), and (13), solves the problem. It is straightforward to show that this is identical to the approximation proposed in reference [12]. Therefore, the discussion of the advantages and disadvantages of the method found therein remains valid. The main disadvantage was clearly the neglect of quasiparticle damping in the *ansatz* (29).

Now turning back to the MAA, its benefits are immediately clear. While reproducing the high-energy expansion up to the same order as the SDA, it additionally incorporates quasiparticle damping via the CPA formalism. And contrary to the conventional alloy analogy, the freedom of defining the 'alloyed components' is used to ensure the correct high-energy expansion (22).

We conclude that the essentials of the qualitatively convincing SDA used in our previous paper [12] are incorporated in the MAA and completed by a proper quasiparticle damping. So the MAA represents a systematic improvement and extension of the SDA. Comparison of results for the MAA and SDA will allow us to inspect very directly the influence of quasiparticle damping on magnetic stability in the PAM.

4. Results and discussion

The theory presented for the periodic Anderson model has been evaluated for a system characterized by the following parameters: the density of states for the free conduction band is chosen to be semi-elliptic with a width of $W = 1$ eV centred at $E = 0$. The f level is determined by its distance (e_f) from the conduction band centre and the intra-atomic Coulomb interaction U. The latter is 4 eV throughout the paper. This means that we consider the PAM in the strong-coupling regime. Furthermore, we are mainly interested in the intermediate-valence regime, i.e. e_f is presumed to be located within the Bloch-band region (-0.5 eV $< e_\mathrm{f} <$ +0.5 eV). It turns out that the physics of the PAM strongly depends on the total particle density

$$n^{(\mathrm{tot})} = \sum_\sigma (n_\sigma^{(\mathrm{f})} + n_\sigma^{(\mathrm{s})}) \qquad 0 \leqslant n^{(\mathrm{tot})} \leqslant 4. \tag{31}$$

We therefore present results for different $n^{(\mathrm{tot})}$, but such that the upper charge excitation at $e_\mathrm{f} + U$ (the 'upper Hubbard band') remains in all cases unoccupied ($n^{(\mathrm{tot})} < 3$). Another decisive variable is of course the temperature T given in K. The evaluation of our theory has been done for a translationally symmetric lattice; antiferromagnetic ordering is not considered. We concentrate instead on the possibility of and the conditions for spontaneous ferromagnetism.

The magnetic phase diagram in terms of $n^{(\mathrm{tot})}$ and e_f for a small hybridization $V = 0.1$ eV is plotted in figure 1. For a given e_f within the Bloch-band region, ferromagnetism becomes possible for particle densities in between a lower and an upper critical value. These critical values shift to higher numbers with increasing f-level position. Ferromagnetism is of course

basically induced by the correlated f electrons. Except as regards the hybridization with the conduction electrons, they are described by the zero-bandwidth Hubbard model. The latter special case, however, forbids ferromagnetism. So a finite hybridization V is needed. On the other hand, one knows that ferromagnetic spin order in the Hubbard model is bound by further conditions: the band occupation and the Coulomb correlation U/W must exceed critical values which are different for different lattice structures [14, 15, 29, 30]. Furthermore, the free band should have an asymmetric density of states [31]. Neither the SDA nor the MAA allows ferromagnetism in the 'pure' Hubbard model for highly symmetric free densities of states such as the semi-elliptic one, irrespective of the correlation strength U/W. In the PAM with finite hybridization V, however, all of these conditions can be met: the hybridization creates a finite width of the f dispersion, and the resulting effective f band turns out to be strongly asymmetric, thereby allowing for a ferromagnetic ground state. For a given e_f, the lower critical density in the phase diagram (figure 1) is the analogue of the critical particle density in the Hubbard model [15]. At the upper boundary, the lower f charge excitation is more or less filled, corresponding to a half-filled band in the strongly coupled Hubbard model for which antiferromagnetism is to be expected [15, 32].

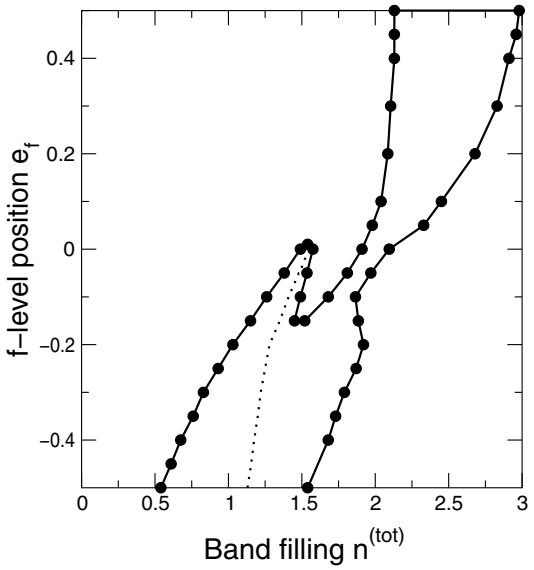

Figure 1. The magnetic phase diagram in the $n^{(tot)}$–e_f plane for $V = 0.1$, $U = 4$, and $T = 0$. f and s magnetizations are parallel to the left of the dotted line and antiparallel to the right.

The upper boundary in the phase diagram for a given e_f always corresponds to a first-order transition, the lower one to a second-order transition. This can be seen in figure 2 where the spontaneous $T = 0$ magnetization is plotted as function of the total particle density $n^{(tot)}$. The position of the f level leads to strikingly different behaviour of the magnetization.

With e_f in the lower half of the conduction band (left column in figure 2), the f magnetization increases from the lower boundary very rapidly to saturation to show the above-mentioned discontinuous transition into the paramagnetic phase at the upper boundary. It is interesting that the induced s polarization is at first positive (ferromagnetic s–f coupling) for weak electron densities, and changes its sign (antiferromagnetic s–f coupling) at about $n^{(tot)} = 1.2$. According to the Schrieffer–Wolff transformation [9], at first glance an antiferromagnetic coupling between s and f electrons would be expected. However, the trans-

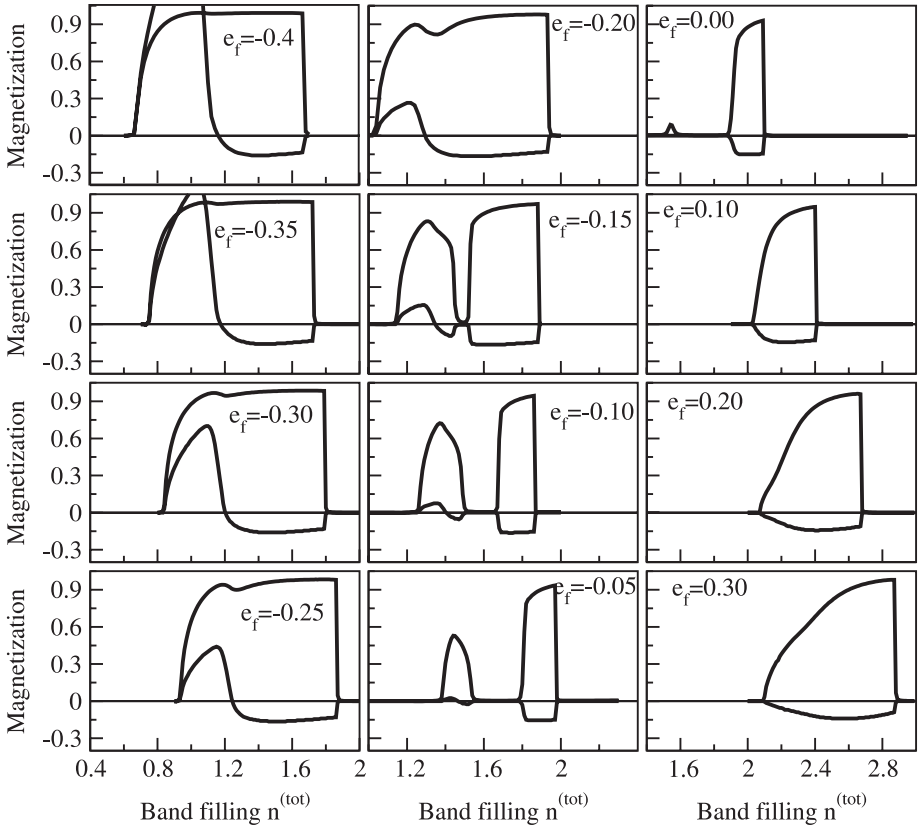

Figure 2. f (solid line) and s (dotted line) magnetizations as functions of $n^{(\mathrm{tot})}$ for various values of e_f. The s magnetization is multiplied by a factor of 5 for better visibility. The other parameters are as for figure 1.

formation is bound by the Kondo limit ($n^{(\mathrm{f})} = 1$) and is not necessarily conclusive for the intermediate-valence region which is investigated here. The quasiparticle density of states (QDOS), plotted in figure 3 for $e_\mathrm{f} = -0.3$ eV and various electron densities, gives some indication of how to understand the sign change of the s-electron polarization. It is instructive to decompose the QDOS into s and f parts, although this decomposition is artificial because of the finite hybridization. The latter takes care of the fact that s and f partial QDOS occupy exactly the same energy regions but of course with different weights. In the $\uparrow$ parts of both spectra the hybridization gap around $e_\mathrm{f} = -0.3$ eV is clearly visible. For practically all densities $n^{(\mathrm{tot})}$ exhibited in figure 3, the f system is saturated, i.e. there are no down-spin f electrons. It is known from the Hubbard model [13, 15], and will be shown in figure 13 for the PAM, that then the damping of up-spin quasiparticles is in such a case negligible compared to that of down-spin quasiparticles. Fine structures like the hybridization gap are to be seen in the up spectrum but not in the down spectrum. The comparison with the SDA results in reference [12] confirms the interpretation that quasiparticle damping closes the hybridization gap in the $\downarrow$ spectrum. The SDA neglects such damping effects; consequently the SDA $\downarrow$ spectrum, too, exhibits a gap. There is a slight exchange shift in the s part due to hybridization. As long as the chemical potential μ is below the hybridization gap, the system contains more up-spin than down-spin s electrons; the s–f coupling is ferromagnetic. When μ shifts above

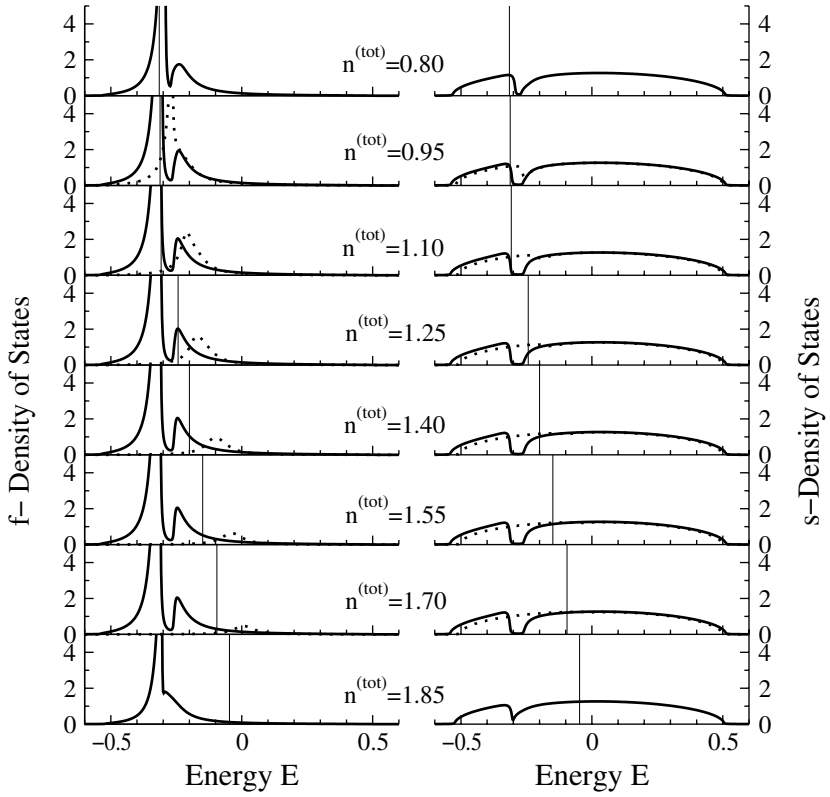

Figure 3. f- and s-quasiparticle densities of states for various values of $n^{(\mathrm{tot})}$ and $e_\mathrm{f} = -0.3$. Full lines are for spin up and dotted lines for spin down. The other parameters are as for figure 1. Thin vertical lines show the positions of the chemical potential.

the gap (in figure 3 in between $n^{(\mathrm{tot})} = 1.10$ and $n^{(\mathrm{tot})} = 1.25$), which exists only in the up spectrum, then the increase in $n_\downarrow^{(\mathrm{s})}$ distinctly exceeds that of $n_\uparrow^{(\mathrm{s})}$, and the s–f coupling becomes antiferromagnetic. That explains the magnetization behaviour in figure 2 (left column) as a density-of-states effect. Note, however, that the absolute value of the induced s polarization is always rather small.

A qualitatively different situation is observed for the magnetization when e_f is near to the centre of the s band (middle column in figure 2). A re-entrant course appears, obviously not connected with the sign change of the s polarization. It manifests itself in the phase diagram of figure 1 by causing 'oscillating' phase boundaries. Again, a look at the respective QDOS is quite instructive. Figure 4 shows the example with $e_\mathrm{f} = -0.1$ eV. For such an f-level position, the hybridization gap splits the f-dominated part of the spectrum rather symmetrically into two almost equally weighted peaks. That holds in particular for the $\uparrow$ spectrum of the ferromagnetic phase ($n^{(\mathrm{tot})} = 1.35, 1.45, 1.75, 1.85$ in figure 4). The chemical potential μ is located in one of the peaks, a situation which according to the simple Stoner criterion favours the appearance of ferromagnetism. As already discussed for the case of figure 3 (left column in figure 2), in the ordered phase $\uparrow$ quasiparticles are rather long-living while the $\downarrow$ particles are strongly damped. Again we conclude that this is why the hybridization gap exists only in the $\uparrow$ spectrum. The spontaneous ferromagnetism disappears when μ enters the hybridization gap, in accordance with the Stoner criterion. The quasiparticles are more strongly damped in the paramagnetic

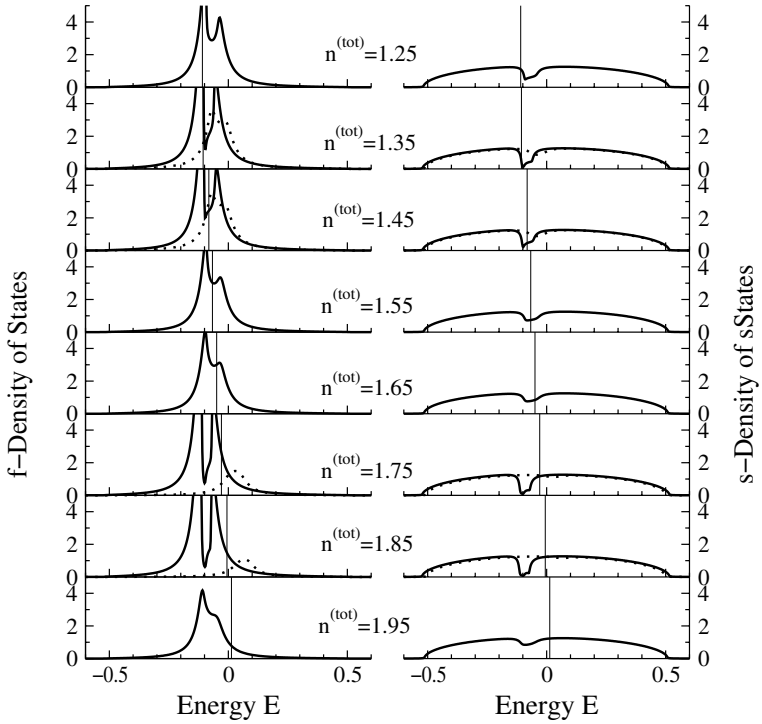

Figure 4. As figure 3, but for $e_f = -0.1$.

phase than the ↑ particles in the ordered phase, so the hybridization gap is more or less covered by the 'smeared-out' quasiparticle peaks.

When the bare f level e_f has been shifted into the upper half of the conduction band, the polarization type changes once more. The coupling between s and f electrons is always antiferromagnetic (right column in figure 2). The QDOS in figure 5, for the case with $e_f = 0.3$ eV, reveals that ferromagnetic order sets in only when μ is above the hybridization gap. The consequence is that there are more s electrons with spin ↓ than with spin ↑.

The phase diagram in figure 1 is calculated for a fixed hybridization $V = 0.1$ eV. It is clear that V has a decisive influence on the extent of the ferromagnetic phase in the e_f–$n^{(tot)}$ plane. Figure 6 demonstrates that the higher the hybridization V, the smaller the ferromagnetic region. On the other hand, the induced polarization of the s electrons increases with growing hybridization. Antiparallel coupling appears only for weak V. Strong electron fluctuations between the s band and f level generally diminish the magnetic stability but enhance the polarization of the s band. However, the same hybridization is exclusively responsible for the ferromagnetic order. For $V = 0$, ferromagnetism is not permitted.

It is interesting to find out to what extent quasiparticle damping may influence the possibility and the stability of ferromagnetic order. This can best be done by a comparison of the results found from the SDA [12] and the MAA. The two methods are based on the same physical ideas; the MAA can be classified as 'the SDA plus quasiparticle damping'. Figure 7 shows the magnetic phase diagrams, derived within the SDA and the MAA for the same set of model parameters. The e_f–$n^{(tot)}$ area of the ferromagnetic phase is distinctly restricted in the MAA because of the quasiparticle damping, in contrast to the SDA result, which is free of damping effects. For both methods we find that for lower particle densities a ferromagnetic and

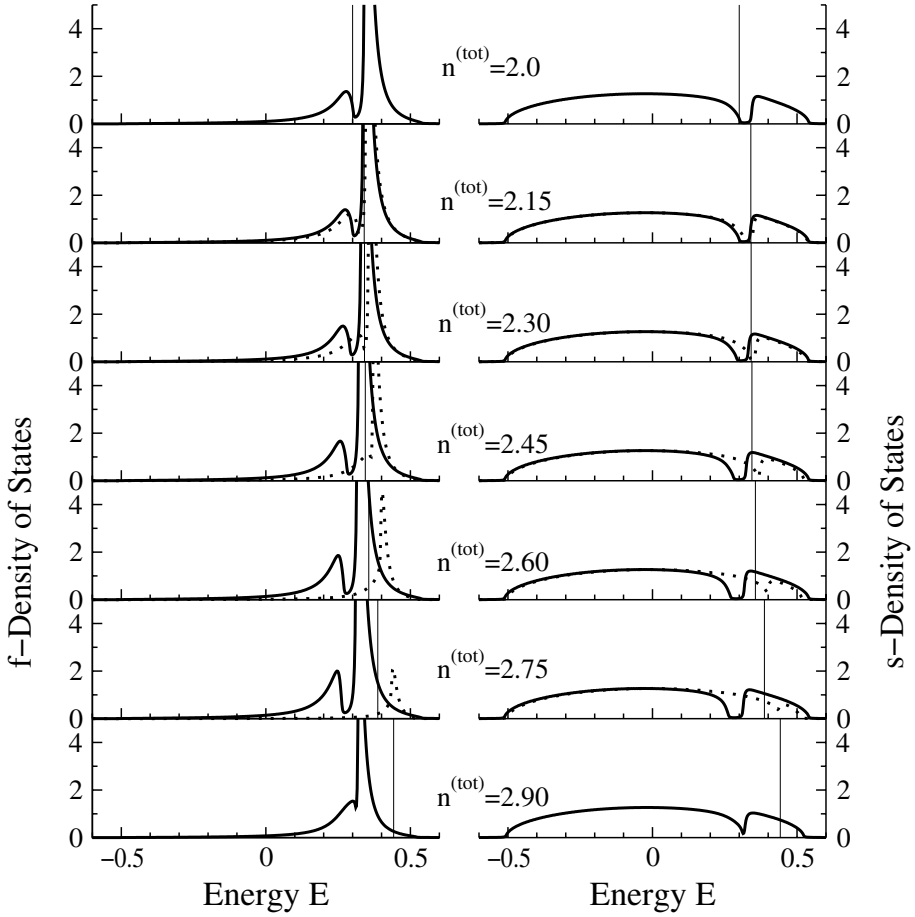

Figure 5. As figure 3, but for $e_f = 0.3$.

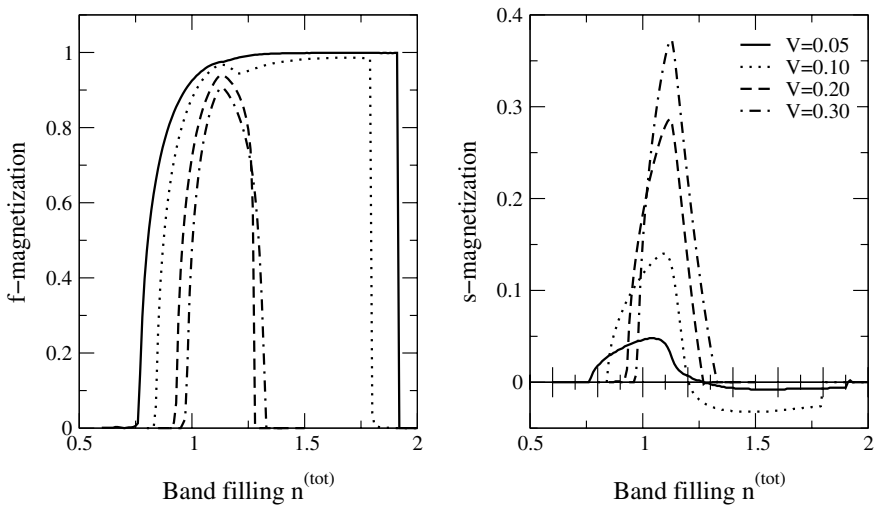

Figure 6. f and s magnetizations as functions of $n^{(tot)}$ for different values of the hybridization strength V with $e_f = -0.3$. The other parameters are as for figure 1.

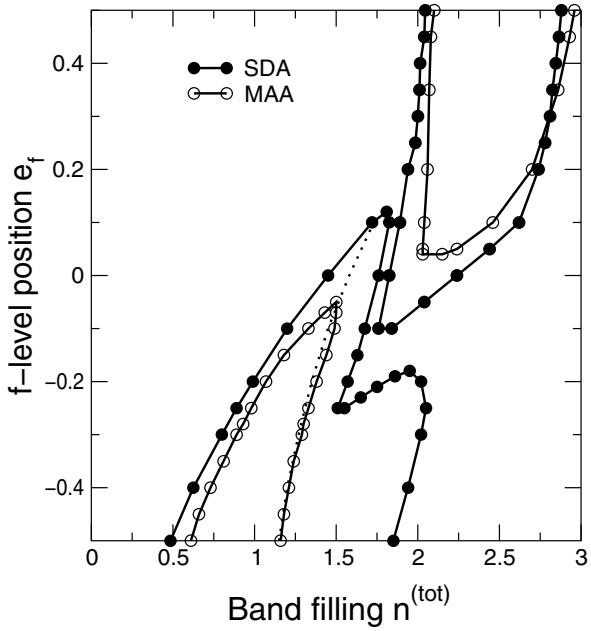

Figure 7. The magnetic phase diagram for the MAA and SDA with $V = 0.2$, $U = 4$, and $T = 0$. The f and s magnetizations are parallel to the left of the dotted line and antiparallel to the right in the SDA. In the MAA the f and s magnetizations are antiparallel only when $n^{(\mathrm{tot})} > 2$.

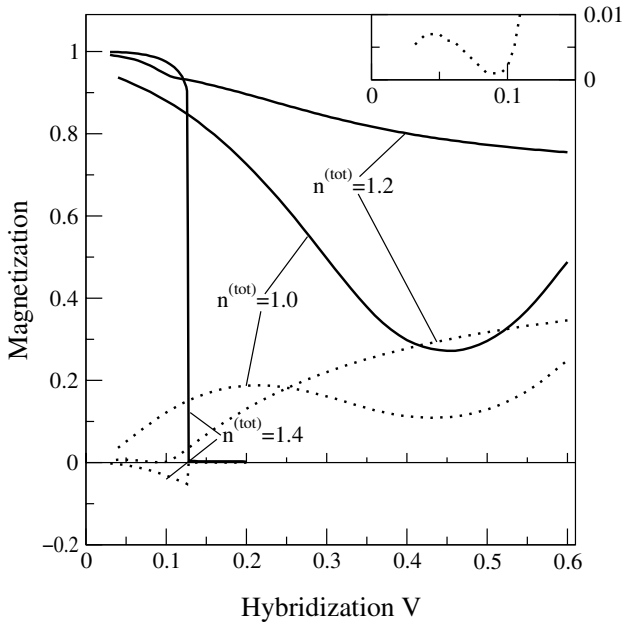

Figure 8. f (solid line) and s (dotted line) magnetizations as functions of the hybridization strength V for different values of $n^{(\mathrm{tot})}$ for $e_\mathrm{f} = -0.3$ at $T = 0$. The inset shows the s magnetization for $n^{(\mathrm{tot})} = 1.2$ in the region of small V.

for higher densities an antiferromagnetic coupling of the s-electron spins to the local f moments takes place.

Up to now we have discussed mainly the e_f- and the $n^{(tot)}$-dependences of the physical properties of the periodic Anderson model. Let us now examine the influence of V in detail. Some results are plotted in figures 8, 9, and 10 for $e_f = -0.3$ eV and several particle densities $n^{(tot)}$. The behaviour is not at all unique. For $n^{(tot)} = 1.4$ a rather weak hybridization V is sufficient to destroy the ferromagnetism (figure 8). The Curie temperature T_c runs through a maximum (figure 9), pointing to the fact that V provokes two competing effects. It broadens the f level, thus creating the precondition for a magnetic order (no ferromagnetism in the zero-bandwidth Hubbard model [30]!) On the other hand, increasing s–f fluctuations must damage the ferromagnetic order because the empty f level does not carry a magnetic moment. It is remarkable that T_c goes smoothly to zero (figure 9) although the $T = 0$ magnetization undergoes a first-order transition (figure 8).

A completely different V-dependence shows up for the band occupations $n^{(tot)} = 1.0$ and 1.2. In these cases large hybridization strength does not destroy the ferromagnetism, but rather enhances T_c. On closely examining figure 8, one recognizes a 'kink' or a minimum in the respective magnetization curves, for $n^{(tot)} = 1.0$ at $V \approx 0.45$ and for $n^{(tot)} = 1.2$ at $V \approx 0.09$. By comparing with the densities of states (figure 10), we note that this value approximately coincides with the V-value where μ enters the hybridization gap in the $\uparrow$ QDOS. That is, the system becomes a semi-metal where only the $\downarrow$ electrons contribute to the electrical current. One might speculate that this has something to do with the increasing T_c. However, we cannot rule out the possibility that this is an effect of our approximation rather than an inherent property of the PAM.

Let us finally discuss the temperature dependence of the magnetic properties, e.g. the spontaneous magnetization (figure 11). First-order as well as second-order transitions appear. Whether first-order transitions are artefacts of our approximate procedure or intrinsic properties of the PAM is not clear. A similar situation is found when applying the MAA to the Hubbard model [24]. In the case of a second-order transition, the f magnetization behaves like a Brillouin function, while the corresponding induced s polarization very often shows remarkable deviations. The examples plotted in figure 11 demonstrate again that the s–f coupling may be ferromagnetic or antiferromagnetic depending on the band filling.

A key quantity of ferromagnetism is the Curie temperature T_c, which is of course decisively influenced by the band filling (figure 12). The $n^{(tot)}$-dependence is very much more regular than the V-dependence exhibited in figure 9. The re-entrant behaviour for $e_f = -0.1$ eV corresponds to that of the $T = 0$ moment in figure 2 (middle column). The calculated T_c-values are of a realistic order of magnitude. The transition into the paramagnetic phase ($T_c = 0$) seems to be always continuous even if the breakdown of the $T = 0$ moment is discontinuous (figure 2). The temperature dependence of the magnetization is due to a corresponding behaviour of the QDOS (figure 13). There is a distinct spin asymmetry in the lower f-like peak ('lower Hubbard band') which causes the spontaneous magnetic moment. The up-spin part is characterized by a hybridization gap, which is not visible in the down-spin spectrum (cf. figures 3, 4, and 5). As already mentioned, this is due to quasiparticle damping, which for low temperatures is very much stronger for $\downarrow$ than for $\uparrow$ quasiparticles (cf. figure 13). With increasing temperature the damping of the $\uparrow$ particles gets larger and that of the $\downarrow$ particles gets smaller. For increasing temperatures, a dip develops in the spin-$\downarrow$ QDOS, which eventually merges with the spin-$\uparrow$ hybridization gap at $T = T_c$. The spin asymmetry is then removed. The induced spin polarization of the conduction band is always very weak, so the assumption that the collective order is based on an RKKY-like coupling via the polarized conduction electrons appears unlikely. It is rather easier to believe that the

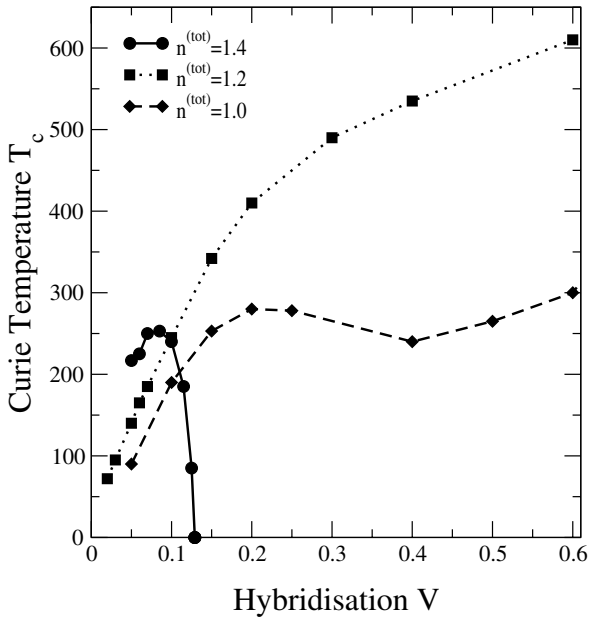

Figure 9. Curie Temperature T_c as a function of V for different values of $n^{(tot)}$ with $e_f = -0.3$.

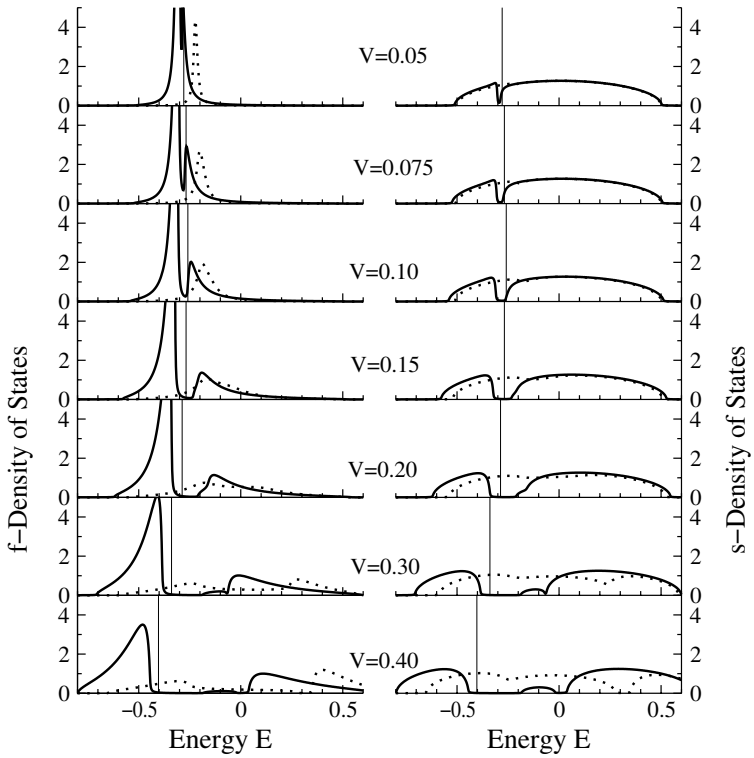

Figure 10. f- and s-quasiparticle densities of states for various values of V with $e_f = -0.3$ and $n^{(tot)} = 1.2$ at $T = 0$. Full lines are for spin up and dotted lines for spin down. Thin vertical lines show the positions of the chemical potential.

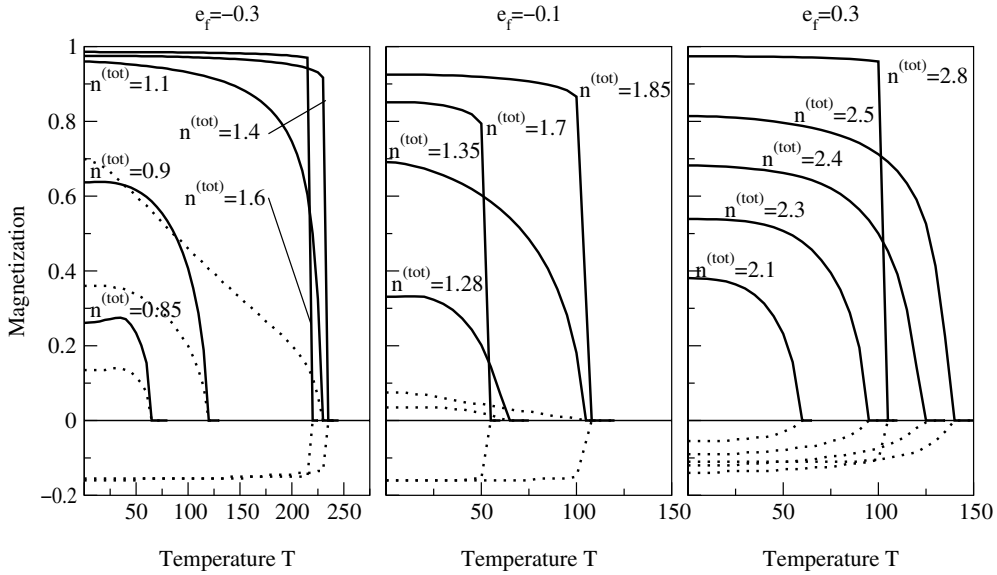

Figure 11. f (solid line) and s (dotted line) magnetizations as functions of temperature for various e_f and $n^{(tot)}$ as indicated in the figure. The s magnetization is multiplied by a factor of 5 for improved clarity.

observed ferromagnetism is due to strong electron correlations in the narrow 'f band', as is the case in the single-band Hubbard model [25, 33]. The coupling to the s band via V takes care of the finite width of the original f level, being in this sense the basic precondition for ferromagnetic order in the periodic Anderson model.

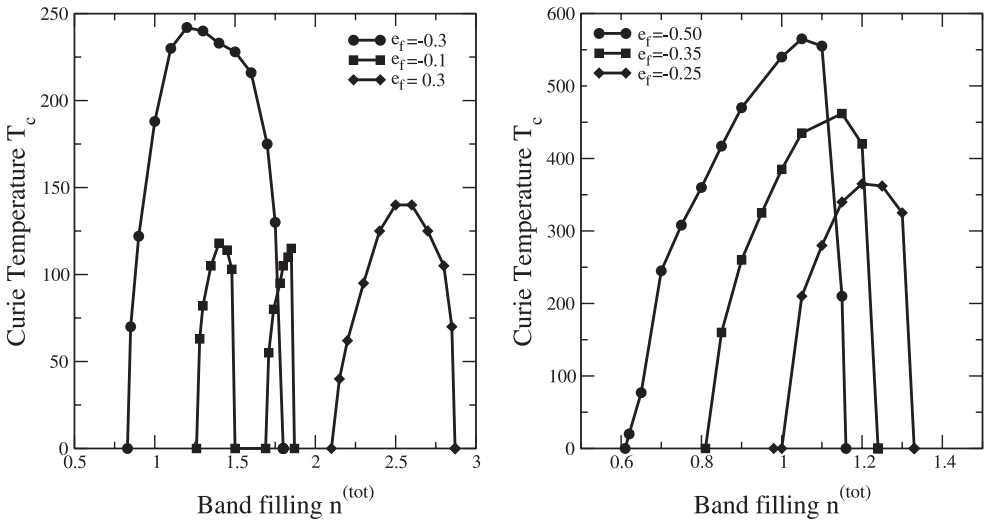

Figure 12. Curie temperature T_c as a function of band filling $n^{(tot)}$ for different values of e_f. The hybridization strength is $V = 0.1$ on the left and $V = 0.2$ on the right.

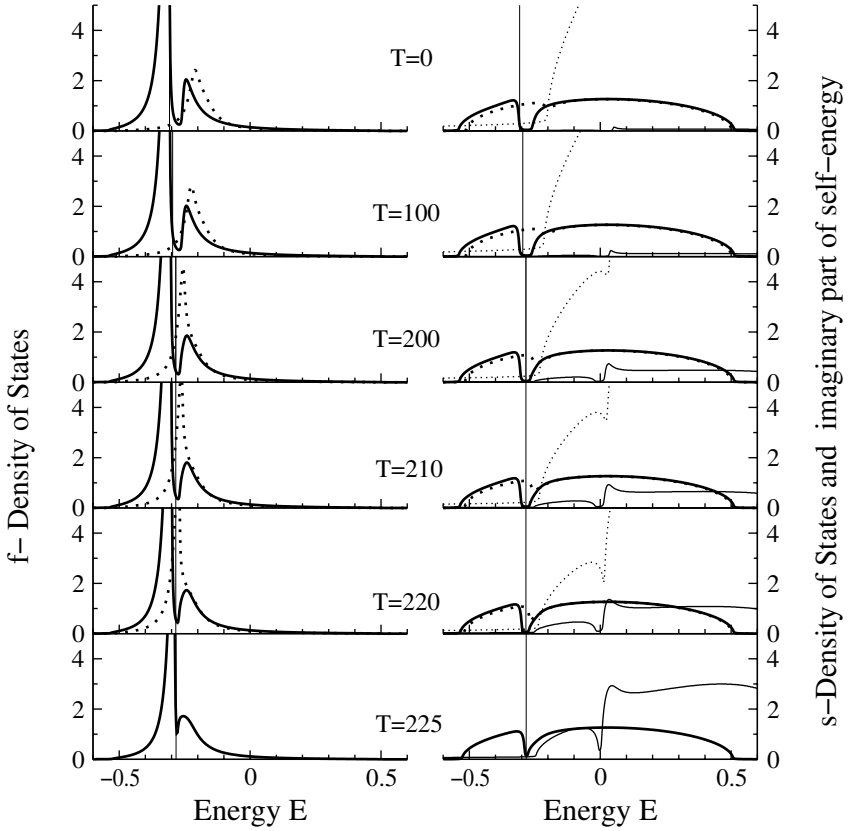

Figure 13. f- and s-quasiparticle densities of states at various temperatures. $e_f = -0.3$, $V = 0.1$, and $n^{(tot)} = 1.1$. Full lines are for spin up and dotted lines for spin down. Thin vertical lines show the positions of the chemical potential. Additionally, the imaginary part of the self-energy is plotted as thin lines in the right-hand column. For better visibility, it is multiplied by -100.

5. Conclusions

A 'modified alloy analogy' (MAA) [24, 25], previously introduced as an approach to the single-band Hubbard model [30], has been applied to the periodic Anderson model (PAM). A high-energy expansion of relevant Green functions and a corresponding expansion of the determining equation for the CPA self-energy have been used to find the optimum alloy analogy for the PAM. This alloy analogy was then used to solve the PAM many-body problem within the CPA. By construction, the MAA represents a strong-coupling approach, and is hence most probably suitable for describing spontaneous ferromagnetism in the PAM. It can be considered as an extension and improvement of the 'spectral density approach' (SDA) [13–15,24]—mainly by inclusion of quasiparticle damping. It cannot, however, reproduce the low-energy features of the PAM (Kondo resonance) [1, 34], being certainly not so decisive as regards magnetic stability. It incorporates, however, important higher correlation functions ('spin-dependent band shift') which guarantee the correct strong-coupling behaviour [21].

The present study focuses on the possibility and the stability of ferromagnetism in the PAM: magnetic phase diagrams are constructed in terms of relevant model parameters such as the hybridization strength V, f-level position e_f, and total particle density $n^{(tot)}$. For this work

we are mainly interested in the intermediate-valence regime, i.e. where e_f is chosen within the energy region of the 'free' Bloch band. The same holds for the chemical potential μ. As usual, the 'f level' and conduction band are assumed to be non-degenerate. The intra-atomic Coulomb interaction U of the f electrons leads to a splitting of e_f into two sublevels at e_f and $e_f + U$. U is chosen such that the upper charge excitation remains unoccupied, i.e. $0 < n^{(tot)} < 3$. The influence of V is multifold. First of all, it leads to a finite width of the lower f-quasiparticle peak that turns out to be a basic prerequisite for ferromagnetism in the intermediate-valence PAM. On the other hand, too strong s–f fluctuations due to V destabilize the ferromagnetic order. Additionally, V induces a hybridization gap in the energy spectrum, which, however, gets closed by too strong quasiparticle damping. If the f magnetization is almost saturated, then the $\uparrow$ spectrum shows a hybridization gap, while the $\downarrow$ spectrum does not. This has some influence on the induced s polarization which can be parallel or antiparallel to the f moment. The Curie temperatures derived are of reasonable orders of magnitude. All of the magnetic properties of the PAM can be illustratively traced back and reasoned out by inspection of the respective quasiparticle densities of states.

Acknowledgments

We wish to thank T Herrmann for very helpful discussions. Financial support by the *Volkswagen-Foundation* within the project *'Phasendiagramm des Kondo-Gitter-Modells'* is gratefully acknowledged. One of us (DM) wants to thank the *Friedrich-Naumann-Foundation* for supporting his work.

References

[1] Hewson A C 1993 *The Kondo Problem to Heavy Fermions* (Cambridge: Cambridge University Press)
[2] Tsvelick A M and Wiegmann P B 1983 *Adv. Phys.* **32** 453
[3] Wilson K 1975 *Rev. Mod. Phys.* **47** 773
[4] Metzner W and Vollhardt D 1989 *Phys. Rev. Lett.* **62** 324
[5] Pruschke T, Jarrell M and Freericks J K 1995 *Adv. Phys.* **44** 187
[6] Georges A, Kotliar G, Krauth W and Rozenberg M J 1996 *Rev. Mod. Phys.* **68** 13
[7] Bulla R, Hewson A C and Pruschke T 1998 *J. Phys.: Condens. Matter* **10** 8365
[8] Meyer D, Wegner T, Potthoff M and Nolting W 1999 *Physica* B **270** 225
[9] Schrieffer J R and Wolff P A 1966 *Phys. Rev.* **149** 491
[10] Doniach S 1977 *Physica* B **91** 231
[11] Ramirez A P 1997 *J. Phys.: Condens. Matter* **9** 8171
[12] Meyer D, Nolting W, Reddy G G and Ramakanth A 1998 *Phys. Status Solidi* b **208** 473
[13] Geipel G and Nolting W 1988 *Phys. Rev.* B **38** 2608
[14] Nolting W and Borgieł W 1989 *Phys. Rev.* B **39** 6962
[15] Herrmann T and Nolting W 1997 *J. Magn. Magn. Mater.* **170** 253
[16] Velicky B, Kirkpatrick S and Ehrenreich H 1968 *Phys. Rev.* **175** 747
[17] Hubbard J 1964 *Proc. R. Soc.* A **281** 401
[18] Leder H J and Czycholl G 1979 *Z. Phys.* B **35** 7
[19] Czycholl G 1986 *Phys. Rep.* **143** 277
[20] Vlamming R and Vollhardt D 1992 *Phys. Rev.* B **45** 4637
[21] Harris A and Lange R 1967 *Phys. Rev.* **157** 295
[22] Bulk G and Jelitto R J 1990 *Phys. Rev.* B **41** 413
[23] Potthoff M and Nolting W 1997 *Z. Phys.* B **104** 265
[24] Potthoff M, Herrmann T, Wegner T and Nolting W 1998 *Phys. Status Solidi* b **210** 199
[25] Herrmann T and Nolting W 1996 *Phys. Rev.* B **53** 10 579
[26] Fukuyama H and Ehrenreich H 1973 *Phys. Rev.* B **7** 3266
[27] Schneider J and Drehel V 1975 *Phys. Status Solidi* b **68** 207
[28] Meyer D and Nolting W 2000 *Physica* B **281** 189

[29] Herrmann T and Nolting W 1999 *Phys. Rev.* B **60** 12 861
[30] Hubbard J 1963 *Proc. R. Soc.* A **276** 238
[31] Wahle J *et al* 1998 *Phys. Rev.* B **58** 12 749
[32] Anderson P W 1963 *Solid State Physics: Advances in Research and Applications* vol 14, ed F Seitz and D Turnbull (New York: Academic) p 99
[33] Herrmann T and Nolting W 1997 *Solid State Commun.* **103** 351
[34] Jarrell M 1995 *Phys. Rev.* B **51** 7429